

PREDICTION OF PARTICLE EROSION IN THE INTERNAL COOLING CHANNELS OF A TURBINE BLADE

D. Anielli - D. Borello - F. Rispoli - A. Salvagni - P. Venturini

Dept. of Mechanical and Aerospace Engineering, Sapienza University of Rome, Rome, Italy

davide.anielli@alice.it, domenico.borello@uniroma1.it, franco.rispoli@uniroma1.it, ales-
sandro.salvagni@uniroma1.it, paolo.venturini@uniroma1.it

ABSTRACT

A multi-phase computational approach was adopted for predicting particle erosion in a domain that is representative of the trailing edge region of a rotor blade. The flow field was solved by an in-house FV code adopting a non-linear k-eps-zeta-f elliptic relaxation RANS turbulence model. The model demonstrated to be able to reproduce the anisotropy of near-wall turbulence and, partly, the influence of streamlines curvature on the turbulent flows. Furthermore, URANS predicted very strong unsteadiness that allowed to reconstruct part of the turbulence spectrum and to identify the relevant frequencies. A Lagrangian particle tracking model was used for predicting particle dispersion and erosion of the solid surfaces. Impact mechanisms was modelled using the Tabakoff model, previously validated by the authors on a number of studies. Two particles classes were investigated (5 and 20 μm). The trajectories of the smallest particles were prone to follow the streamlines pattern and erosion rates are also influenced by impact angle. As for the greater particles, the erosion mechanism is mainly dependent from inertia forces.

NOMENCLATURE

C_D	drag coefficient	T	temperature, period
C_μ	eddy-viscosity coefficient	U_i	mean velocity
CFL	Courant-Friedrichs-Lewy number	$u_i u_j$	kinematic Reynolds stress tensor
ER	Erosion rate	\bar{u}	gas velocity vector
f	intermediate variable, Eq.(4)	\bar{v}	particle velocity vector
FFT	Fast Fourier Transform		
\bar{g}	gravity force	<i>Greek</i>	
k	turbulent kinetic energy	α	impact angle
K_i	constants of the erosion model	δ_{ij}	Kronecker delta
L	turbulent length scale	ε	dissipation rate of k
P	mean shear generation rate of k	ζ	ratio between v^2 and k
R_T	tangential restitution coefficient	η_i	non-dimensional velocity gradient in-variant
Re	Reynolds number	ν	kinematic viscosity
S_{ij}	mean rate of strain tensor	ν_t	eddy viscosity
S^*_{ij}	non-dimensional strain rate tensor	ρ_f	fluid density
S	mean shear rate	ρ_p	particle density
SAS	scale-adaptive simulation	τ	turbulent time scale
SIMPLE	Semi-implicit Method for Pressure linked Equations	Ω_{ij}	mean intrinsic vorticity tensor

INTRODUCTION

Increasing the turbine inlet temperature results in an increase of the turbine efficiency, then this is a goal that all manufacturers are continuously trying to achieve. Then, first stages of turbine blades and vanes need to be cooled to maintain the proper mechanical properties even at those temperatures, avoiding turbine structural problems and malfunctioning. The study of flow motion within the internal cooling channels, therefore, represents an actual argument for the improvement of turbine efficiency.

Heat removal from the blade is generally augmented by turbulence promoters placed inside the internal cooling channels. These promoters have different shapes (cylinders, bumps, etc.) and can be displaced with different arrangements [1]. These objects can be used also for structural reasons. On the other hand, their presence increase the pressure losses. Here we consider the presence of oblong pin fins called pedestals; their number and position have to be carefully analyzed in order to obtain the best trade-off between increase of heat transfer and minimization of pressure losses added by the use of pedestals.

The cooling air flowing inside such channels is subjected to several phenomena such as unsteadiness, strong streamlines deviation, rotation, heat transfer. Furthermore, some fouling particles, ingested from the external atmosphere, can cross the entire compressor, mixing with the particles generated by compressor blades erosion and eventually reach the internal cooling channels of the turbine blade. Such channels are very narrow and then no inspection is possible during the blade operating life to check the occurrence of erosion inside the blade. This phenomenon, enhanced by the turbulent and unsteady behavior of the flow itself, can lead to a change in the geometry of the channel hence affecting the operating conditions of the blades. It is important to note that often a large deposit speeds up the erosion process provoking turbine failure or requiring frequent stops for maintenance [2].

Since the internal cooling channels are relatively small, it is not easy to carry out proper experimental tests. It is then worth to perform proper computational campaign, to reproduce the transport and spreading of the solid particles evolving inside the internal cooling vanes. To this end, a proper simulation of the particle laden flow must be carried out. The basic approach for such class of analysis is to integrate a CFD (Eulerian) analysis of the carrier flow with a particle-tracking (Lagrangian) study of the solid particles dispersed in the fluid [3].

Generally, in turbomachinery applications simplified models were adopted. Such models were developed using very crude assumptions (mainly basic RANS closures) to reduce computational costs and improve code numerical stability ([4], [5]). Then, only a qualitative agreement with real conditions is obtained and CFD results must be complemented with experimental tests.

On the contrary, the adoption of physically sound models, able to recover the main turbulent features (unsteadiness, anisotropy, etc.) at a reasonable computational cost can represent a valuable instrument for reducing costs for experimental tests and obtaining accurate clues for improving design methodology. Here we propose the adoption of an unsteady, non-linear version of an elliptic relaxation turbulence model ($k-\varepsilon-\zeta-f$ see [6]). This model was developed by some of the authors to merge the basic capabilities of the elliptic-relaxation model – proper treatment of the near-wall turbulence without damping functions – with the adoption of a non-linear approach to take into account the influence of turbulence anisotropy. The finite volume code T-FlowS, currently developed in our research group at Sapienza was used for the present computations.

The model is here applied to the analysis of the final portion of the cooling channels in the trailing edge region where 7 pedestals were placed. Borello et al. [7] analyzed the flow and heat transfer in a similar test case when the flow is subjected to a solid body rotation. There, the well-known SAS model was used for flow prediction. One of the two side walls was heated. Recently, Borello et al. [8] analyzed the deposit mechanism adopting the same flow modelling. The computational domain reproduces an experimental test case and comparisons with experimental results are presented. From the analysis of unsteady flow we noticed the existence of periodicity probably related to the release of vortical structures from the pedestals. An unsteady Lagrangian model, developed and used by the authors in a number of previous studies (see for instance [3], [6], [8]-[10]), is here used for tracking the particles motion, and the Tabakoff approach [11] is applied for predicting the erosion mechanism.

The same erosion model was used by some of the authors in previous works [12]-[14], obtaining results in fair agreement with available experimental data.

In the next paragraph, we describe the mathematical models of flow modelling and particles tracking and erosion. Then the present case will be described and finally the flow and particle motion in the trailing edge are discussed. Conclusions will close the paper.

MATHEMATICAL MODEL

Flow model

The mathematical flow model here adopted for describing the flow motion is an original, non-linear, incompressible k- ε - ζ -f, low-Reynolds URANS equations set (1-6).

$$\frac{Dk}{Dt} = P + G - \varepsilon + \frac{\partial}{\partial x_j} \left[\left(\nu + \frac{\nu_t}{\sigma_k} \right) \frac{\partial k}{\partial x_j} \right] \quad (1)$$

$$\frac{D\varepsilon}{Dt} = (C_{\varepsilon 1} P + C_{\varepsilon 3} G - C_{\varepsilon 2} \varepsilon) \frac{\varepsilon}{k} + \frac{\partial}{\partial x_j} \left(\nu + \frac{\nu_t}{\sigma_\varepsilon} \frac{\partial \varepsilon}{\partial x_j} \right) \quad (2)$$

$$\frac{D\zeta}{Dt} = f - \frac{\zeta}{k} P + \frac{\partial}{\partial x_k} \left[\left(\nu + \frac{\nu_t}{\sigma_\zeta} \right) \frac{\partial \zeta}{\partial x_k} \right] \quad (3)$$

$$L^2 \frac{\partial^2 f}{\partial x_j \partial x_j} - f = \frac{C_1}{\tau} \left(\frac{\nu^2}{k} - \frac{2}{3} \right) - C_2 \frac{P}{k} \quad (4)$$

$$\overline{u_i u_j} = \frac{2}{3} k \delta_{ij} - 2C_{\mu 1} \zeta k \tau_1 S_{ij} - \mathcal{Y} k \tau^2 \left[C_{\mu 2} (S_{ik} \Omega_{kj}^* + S_{jk} \Omega_{ki}^*) - C_{\mu 3} \left(S_{ik} S_{kj} - \frac{1}{3} |S|^2 \delta_{ij} \right) \right] \quad (5)$$

$$\tau = \tau_1 = \max \left[\min \left(\frac{k}{\varepsilon}, \frac{2}{3C_{\mu 1} \zeta} \sqrt{\frac{3}{8|S|^2}} \right), 6 \left(\frac{\nu}{\varepsilon} \right)^{0.5} \right] \quad (6)$$

where

$$\Omega_{ij}^* = \Omega_{ij} + 2.25 \varepsilon_{ijk} \Omega_k, \quad \mathcal{Y} = \max \left[\frac{2}{3} - \zeta, 0 \right], \quad C_{\mu 1} = 0.21, \quad C_{\mu 2} = \frac{6}{5} \sqrt{\frac{1 - \left(C_{\mu 1} \frac{\nu^2}{k} \right)^2}{\beta_1 + \sqrt{\eta_1 \eta_2}}} 2\eta_1, \quad C_{\mu 3} = \frac{6}{5(\mathcal{Y} + \eta_1)}, \quad \mathcal{Y} = \frac{1}{0.1 + \eta_1},$$

$$\eta_1 = \tau^2 S_{ik} S_{ik}, \quad \eta_2 = \tau^2 \Omega_{ik} \Omega_{ik}, \quad \beta_1 = \frac{1}{0.1 + \sqrt{\eta_1 \eta_2}}, \quad C_{\varepsilon 1} = 1.44, \quad C_{\varepsilon 2} = 1.92$$

P and G represent turbulent kinetic energy production due to strain and body force respectively, while L and τ are the turbulent length and time scales. The basic model formulation and the rationale are reported in [15], while the non-linear extension was obtained starting from the quadratic formulation of the ν^2 -f model of Petterson Reif [16],[17]. This paper represents the second step (in the first we analysed deposit [6]) of a wider research project aiming at studying heat transfer, particle deposit and erosion in the internal cooling channels of a rotating turbine blade. For such reasons, the model was developed aiming at accounting for all the cited phenomena, although not all of them (e.g. rotation) are considered here.

Particle motion

Particle concentration in a two-phase flow can be measured by the particle volume fraction that is the ratio between particle volume and a unit volume of flow. In turbomachinery applications this ratio is usually small (i.e., less than 1.0^{-6}). With such a concentration, particle-particle collisions are very

rare, thus their contribution on particle motion can be neglected. Moreover, the effect of the particles on the flow motion is also negligible due to the small particle volume fraction. Due to these considerations here we adopt an one-way coupling approach, that is particle motion is only driven by flow motion, but the flow behaves as if the particles are not present.

In this framework, the particle motion is computed by using a Lagrangian approach resolving the equation of particles motion, i.e., the Basset-Boussinesque-Oseen ordinary differential equation. In this kind of applications the only relevant force acting on particles is the drag [18], then the BBO equations can be reduced as follows

$$\rho_p \frac{d\vec{v}}{dt} = -\frac{3}{4d_p} \rho_f C_D (\vec{v} - \vec{u}) |\vec{v} - \vec{u}| + (\rho_p - \rho_f) \vec{g} \quad (1)$$

where C_D is the particle drag coefficient. Such coefficient is evaluated using the Shiller and Naumann expression [18]

$$C_D = \frac{24}{\text{Re}_p} (1 + 0.15 \text{Re}_p^{0.687}) \quad (2)$$

which is valid for particle Reynolds number (Re_p) up to 1000.

Erosion model

According to their experiments, Tabackoff et al. [11] developed an empirical correlation for predicting the erosion per unit mass of impacting particles (ER, in mg/g) of different materials. In their model, they consider the main parameters affecting erosion: impact angle and velocity, and material properties of both particles and target surface. Moreover, the model accounts for the particle shape. The ER is calculated as

$$ER = K_1 f_\alpha |\mathbf{v}_{bc}|^2 \cos^2 \alpha (1 - R_T^2) + f_i \quad (3)$$

with

$$R_T = 1 - 0.0061 |\mathbf{v}_{bc}| \sin \alpha$$

$$f_\alpha = \left\{ 1 + K_C \left[K_{12} \sin(90\alpha/\alpha_0) \right] \right\}^2$$

$$f_i = K_2 (|\mathbf{v}_{bc}| \sin \alpha)^4$$

where K_1 , K_2 and K_C are functions of material properties of particles and target surface, and α is the impact angle, evaluated with reference to the wall (i.e., normal impact has $\alpha = 90$ degrees). We assume that the channel walls are made of stainless steel. It is worth noting that actual turbine blades are usually made of Ni-Cr superalloys and not stainless steel. However, both these materials are ductile, thus their behaviour to erosion is similar, showing a maximum erosion rate at an impact angle about 30 degrees. It result in a similar erosion patterns but different erosion rate. In order to make the present results as much independent as possible of the blade material, they will be normalized with respect to the maximum value. According to the above assumption, Table 1 shows the material coefficients for stainless steel needed by the model [11], assuming an angle of maximum erosion, α_0 , equal to 30 degrees.

Table 1. Erosion model coefficients [11].

K_C	$\alpha \leq 3 \alpha_0$	1
	$\alpha > 3 \alpha_0$	0
K_1		$1.505101 \cdot 10^{-06}$
K_{12}		$2.96077 \cdot 10^{-01}$
K_2		$5.0 \cdot 10^{-12}$

COMPUTATIONAL DETAILS

The configuration here analysed reproduces the trailing edge region of the cooling blade. In Figure 1 we show the computational domain with inlet and outlet sections and the grid. The work reproduces the experiments of Bianchini et al. [1].

The grid consists of 4.5 M Hexahedral cells. A rounded edge was introduced to model the region indicated with a red circle in Figure 1-left and magnified in Figure 1-right top. Boundary conditions adopted in the present simulations, are reported in Table 2. Inlet temperature and velocity are set according to the experiments [1].

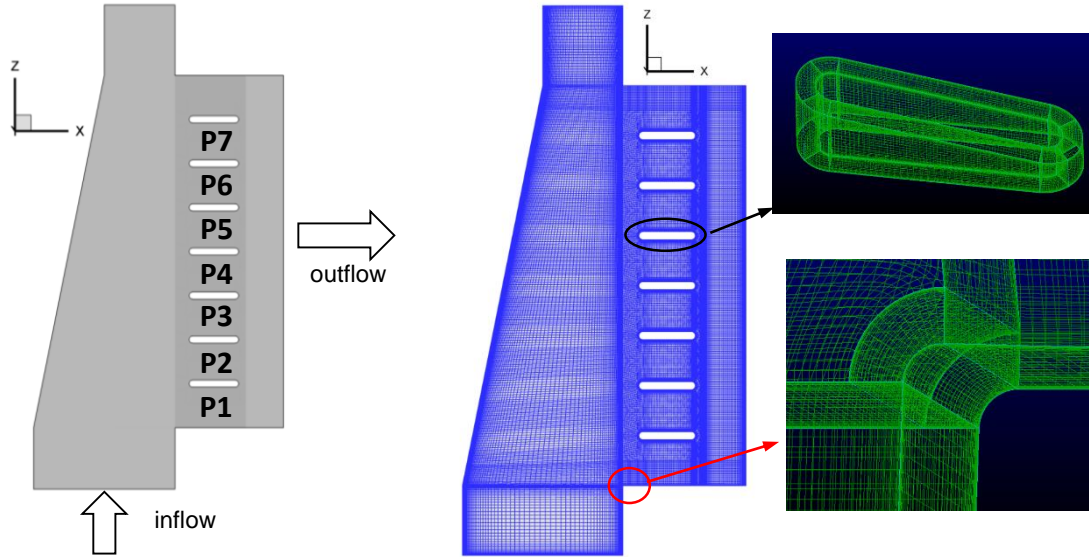


Figure 1. Computational domain: sketch of the domain (left); computational grid (right).

Table 2. Boundary conditions.

Inlet	Outlet	Wall	Heated wall
U=5.3 m/s, T=300 K	Zero-gradient	No-slip, adiabatic	No-slip, T= 340 K

The Reynolds number is calculated on the basis of air properties hydraulic diameter of the inlet section, and inflow velocity and it is equal to 20,000. The inlet turbulent intensity is assumed equal to 3% and the ratio of turbulent and molecular viscosity in inlet is set equal to 10.

The SMART algorithm is adopted to control the instabilities of the convective terms in the governing equations. Time marching solution is obtained using a second-order accurate scheme imposing that the time step was small enough to ensure that the maximum CFL number was always lower than 1. The Navier-Stokes coupled system was solved by using the SIMPLE algorithm.

To account for flow unsteadiness in the particle tracking algorithm, the main period of flow fluctuation is divided into 24 intervals. For any of such intervals a different flow realization is considered as carrier flow for the dispersed particles.

Particle transport and erosion are simulated using P-Track, a Finite-Element-based in-house code developed by the authors at Sapienza Università di Roma [10]. To properly account for particle dynamics, the channel is scaled down from the experimental case to a realistic size (i.e., 5 cm in z direction) keeping the Reynolds number constant.

With the aim of studying the effect of flow fluctuations on particle motion just tracking a small (but statistically relevant) number of particles, some cells have been chosen to seed particles. The selected cells are distributed on six different lines at the inlet surface, named S1-S6 and reported in Figure 2. 80 spherical, non-rotating and non-reacting particles are seeded in each starting cell and at

each new realization, globally simulating more than 382000 particles. Particle properties are reported in Table 3.

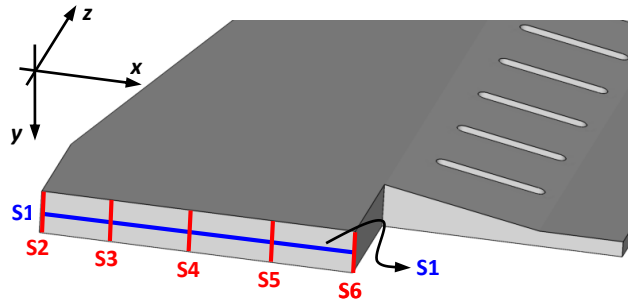


Figure 2. Sections where particles enter the domain.

Table 3. Particle properties.

$d_p(\mu\text{m})$	$\rho_p(\text{kg/m}^3)$	$U_{in}(\text{m/s})$
5, 20	1500	Flow velocity

RESULTS

Flow field

The quality of the predicted velocity field was assessed in a previous paper [6] and it is not discussed here. However, in Figure 3 a comparison of the velocity field computed and measured along a line obtained by the intersection of two reference planes (1-4) is reported. Reference planes are also shown in Figure 3. Plane 1 is parallel to the heated wall and it is placed at 25% of passage height in y direction. Plane 4 is x-normal and it is located at mid of the pedestal length.

It is worth noting that the model adopted allows to properly reproduce the near wall behaviour when compared with baseline RANS model [6](i.e., see the region having abscissa between 0 and 0.05, where a large separation bubble is present). This is due to the introduction of the quadratic term in the formulation, which makes the model able to reproduce the anisotropy of turbulence close to the walls.

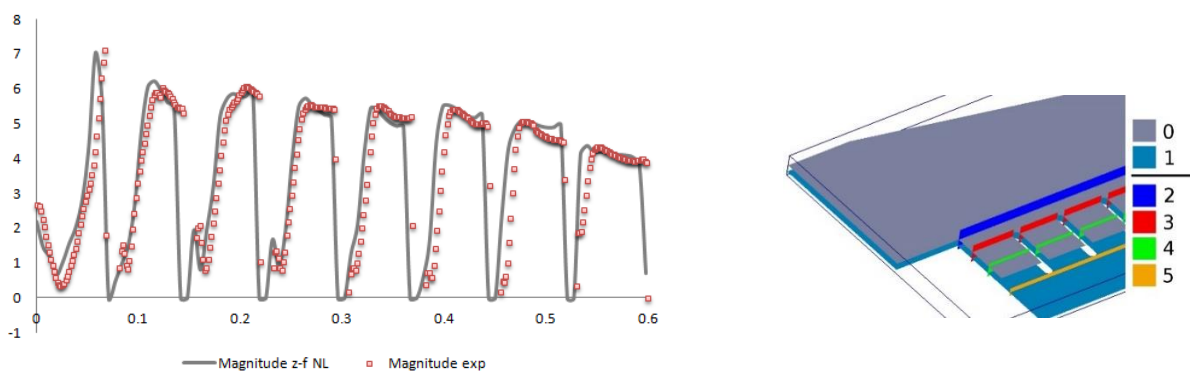


Figure 3. Left: Velocity magnitude in section 14: dots-experiments, lines-computations; right: Reference planes with colour keys. Reference lines cited in the text correspond to the intersection of these planes (e.g. line 03 is the intersection of planes 0 and 3).

Figure 4 shows streamlines and velocity magnitude in plane 1 (see Figure 3-right for planes positions). The velocity increases when moving towards the outlet, where the height of the passing section decreases. Moreover, blow-ups of the region close to the lower wall and the first two pedestals

demonstrate that a recirculation occurs where strong flow deviations are in play. This will surely affect the particle motion.

The presence of large secondary flows suggests that strong unsteadiness takes place. Analysis of fluctuating velocity in a number of monitoring point distributed along the pedestals is presented in Figure 5. We considered the points that are placed above the recirculation bubbles close to the pedestals (yellow rectangle in Figure 5-right) and in the large recirculation bubble (blue square in Figure 5-right).

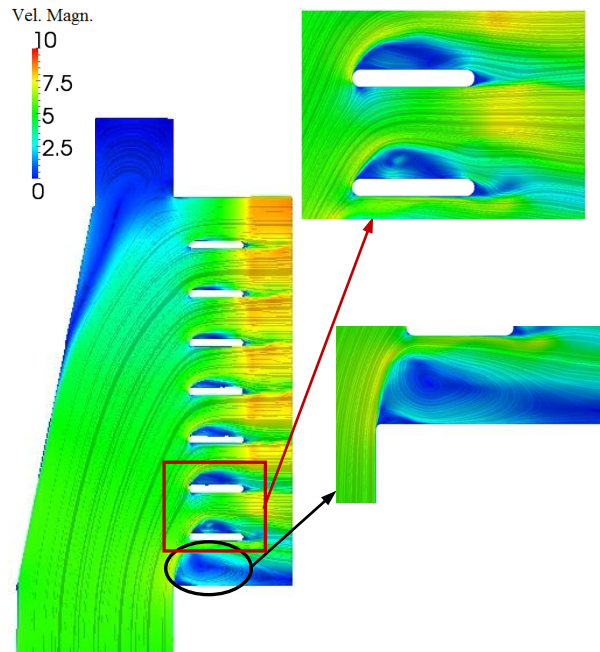


Figure 4. Velocity magnitude and streamlines in plane 1 (see Figure 3-right) for the non-linear ζ -f case; left: whole domain; right: details of the recirculation regions.

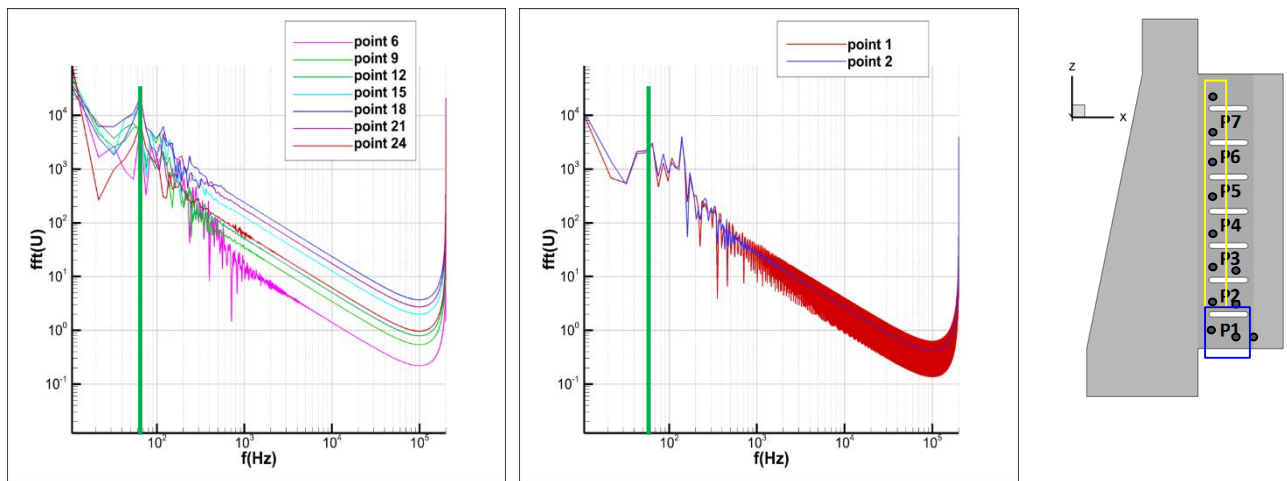


Figure 5. Left - FFT of the unsteady velocity in several points close to the pedestals and on plane 0; centre – FFT of the unsteady velocity in the recirculation bubble (in blue square, right) on plane 0 and plane 1 (see Figure 3-right); right – position of the monitoring point.

From the analysis of the FFT of the velocity fluctuation, it is possible to see that a common peak was obtained for the monitoring points located close to the small recirculation bubbles over the pedestals (Figure 5 left). Moreover, the same peak is present in the recirculation bubble in two

positions placed in Planes 0 and 1 (Figure 5, centre). Starting from this value, we calculated the period of the unsteady motion starting from this value. The resulting period T is equal to 0.19 s and the corresponding Strohal number is equal to 0.22.

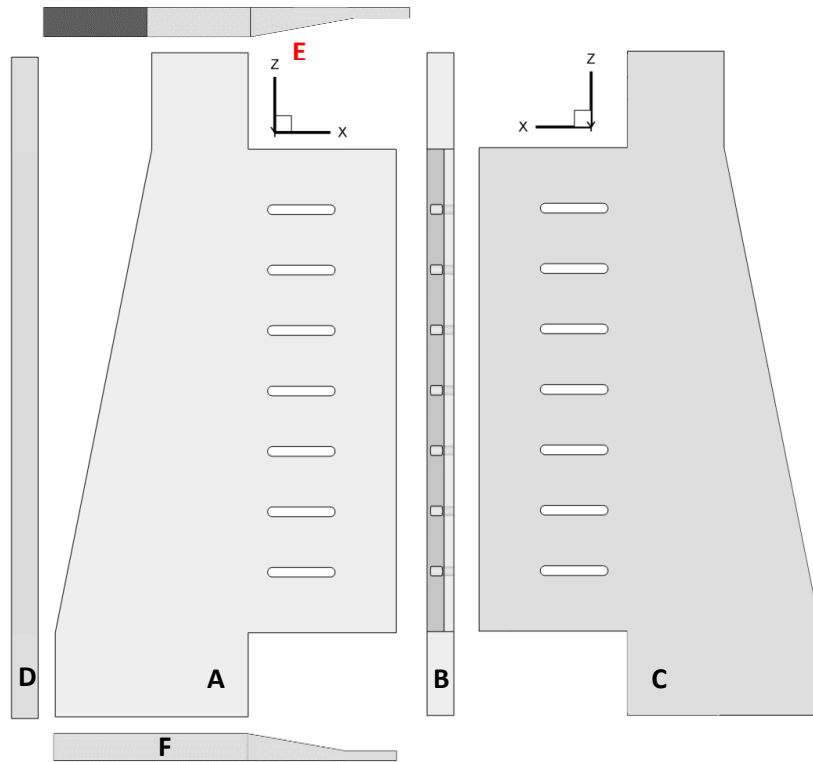


Figure 6 – Reference view planes (A-F).

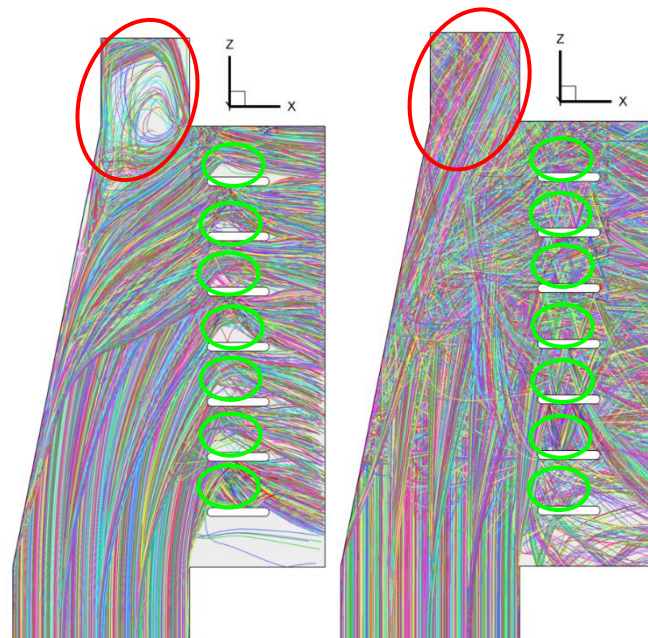


Figure 7. Trajectories of some 5 (left) and 20 (right) μm particles.

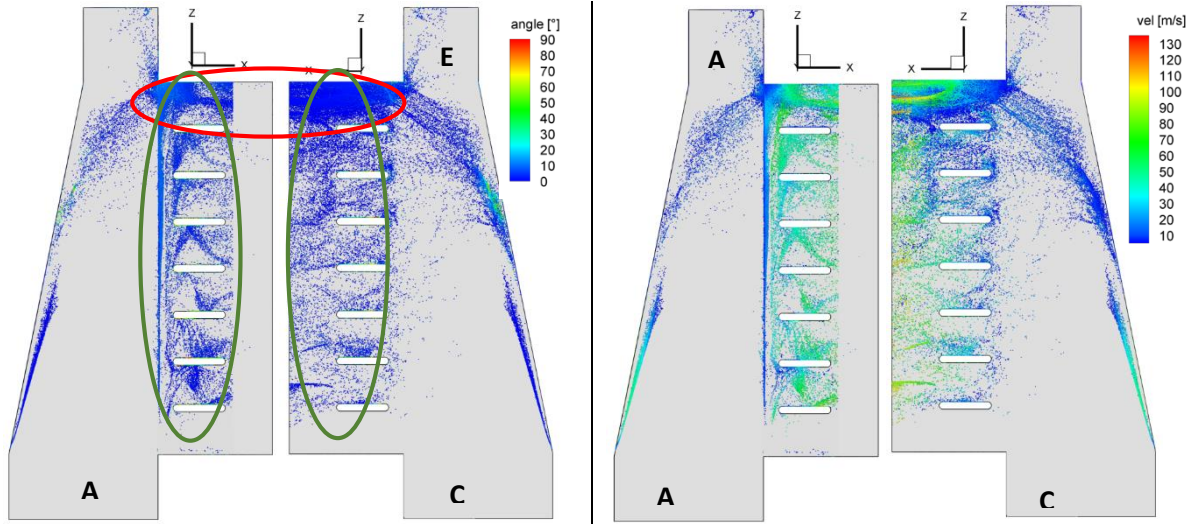


Figure 8. Particle size 5 μm : impact angles (left), and impact velocities (right).

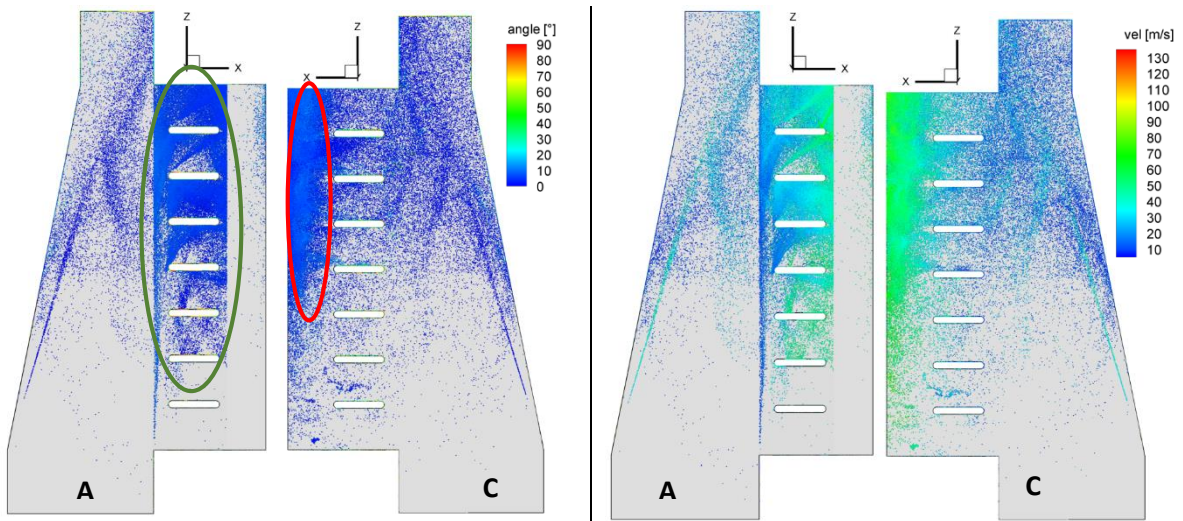


Figure 9. Particle size 20 μm : impact angles (left), and impact velocities (right).

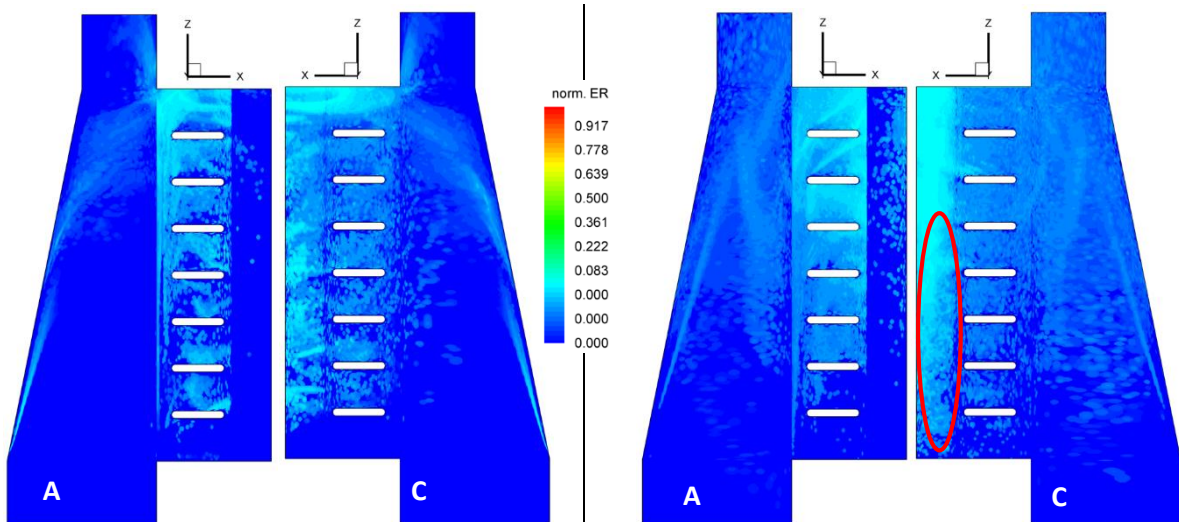


Figure 10. Normalized Erosion rate: 5 μm (left) and 20 μm (right) particles.

Assuming this value, we performed computations for a further period extracting 24 flow realizations (one any 15°). These 24 realizations are used to properly update the flow field governing particles trajectories, thus accounting for flow unsteadiness in particles motion.

Particle tracking and erosion

Here, we are interested to investigate the effect of inertia in particle motion and erosion pattern. This is done simulating two particle size classes, as already reported in Table 3. Figure 6 shows the view planes used in the discussion. View planes A and C are parallel to the xz coordinate plane, seen from $y < 0$ and $y > 0$, respectively; view planes B and D are parallel to yz coordinate plane, seen from $x > 0$ and $x < 0$, respectively; view plane E and F are parallel to the xy coordinate plane, seen from $z > 0$ and $z < 0$, respectively.

Figure 7 shows some particle trajectories. As expected, smaller particles closely follow the streamlines; 20 μm particles on the contrary, have a larger inertia and they tend to follow a more straight trajectories, undergoing several rebounds before leaving the exit section (in this simulation it is assumed that particles elastically rebound on a solid wall). It is worth noting that 5 μm particles are captured by the large recirculation region at the top of the channel (red ellipses), while the larger ones have a large inertia preventing them from being entrapped. Thus, they rebound on the walls and eventually leave the region. As a result, larger particles enter the recirculation region but impact the walls and rebound, being very little affected by the flow fluctuations. For the same reason, smaller particles are also affected by the small recirculation bubbles (green ellipses) forming at the top of pedestals, while larger particles seem to be not affected at all. Due to the large number of impacts and rebounds, the motion of 20 μm particles is more chaotic, and particles are widely spread within the channel. On the contrary, 5 μm particles are spread just in the recirculation regions highlighted in Figure 7, and close to the outlet, where flow fluctuations are very strong. All these effects will contribute to the erosion patterns.

Figure 8 and Figure 9 show impact angles and velocities for 5 μm and 20 μm particles. It is evident that 5 μm particles undergo a smaller number of impacts in comparison to 20 μm particles. Moreover their impacts are mostly concentrated in the upper part of the outlet region of the channel (red ellipse, Figure 8), and in the pedestal region (green ellipse, same figure). The average impact angles in these regions are in the range $0-15^\circ$, and the impact velocities are in 40-80 m/s. Larger particles (Figure 9) also impact the pedestal region, but mostly from pedestal P1 to P4 (green ellipse). It is worth noting that in the view plane C, these particles impact the outlet region mainly after the pedestals (red ellipse). This is due to the fact that particles rebounding the upper part of the pedestal region (view plane A), which is convergent, go towards the opposite wall, continuing their motion to the outlet. It results in a new rebounding region on plane C just after the pedestals and before the outlet. The average impact angles are similar to those of smaller particles, but the impact velocities are a bit larger (60-90 m/s).

Figure 10 shows the normalised erosion rate for 5 μm and 20 μm particles (left and right, respectively). It is evident that in the case of larger particles the channel is more exposed to erosion, showing high values of ER in a wide region of it. It is worth noting the combined effect of impact angles and velocities, especially in the case of smaller particles. Comparing Figure 10 right and Figure 9, it comes out that the region in red ellipse in Figure 10 where ER is quite high, does not correspond to a large number of impacts, thus here the erosion is due to the combination of impact angle and velocity (Figure 9).

CONCLUSIONS

In the present work the authors presented a numerical prediction of erosion on the walls of a channel for internal cooling of a turbine blade. The aim is studying the effect of particle inertia on their motion, and on the erosion patterns. In the study it is also shown the impact angle and velocities of involved regions. Simulations predicted that the regions most exposed to erosion are, for both the particle size classes, that of pedestals and that just after them, close to the outlet, especially for larger particles and on plane C. Apart from these regions, it is clear that larger particles erode a wider part of the channel, and this can be ascribed to the large number of rebounds that those particles undergo. It is worth noting that assuming elastic impacts for particles, results in an overestimation of the erosion since after impact particles rebound with the same kinetic energy. Thus, in possible subsequent impact its impact velocity is likely larger than in a real situation.

REFERENCES

- [1]. Bianchini, B., Simonetti, F., Tarchi, L., Facchini, B., Zecchi, 2012, "Numerical and experimental investigation of turning flow effects on innovative pin fin arrangements for trailing edge cooling configurations", *Journal of Turbomachinery* Vol. 134, Iss.2, 021005 doi:10.1115/1.4003230.
- [2]. Dunn M.G., Baran A.J., Miatech J., 1996, "Operation of Gas Turbine Engines in Volcanic Ash Clouds", *Journal of Engineering for Gas Turbines and Power*, vol.118, pp 724-731.
- [3]. Venturini P., Borello D., Hanjalić K., Rispoli F., 2012, "Modelling of particle deposition in an environment relevant to solid fuel boilers", *Applied Thermal Engineering* 49, pp. 131-138.
- [4]. Donahoo, E. E., Kulkarni, A. K., Belegundu, A. D., and Camci, C., 2001. "Determination of Optimal Row Spacing for a Staggered Cross-Pin Array in a Turbine Blade Cooling Passage". *J. Enhanced Heat Transfer* vol. 8, pp. 41-53.
- [5]. Hamilton, L. J., Adametz, D. S., Lind, E. K., and Gropinath, A., 2002. "Numerical Analysis of the Performance of a Staggered Cross-Pin Array Heat Exchanger". *The Eighth AIAA/ASME Joint Thermophysics and Heat Transfer Conference*.
- [6]. Borello D., Capobianchi P., De Petris M., Rispoli F., Venturini P., "Unsteady RANS analysis of particles deposition in the coolant channel of a gas turbine blade using a non-linear model", *ASME Turbo Expo 2014, Dusseldorf, Germany*, paper no. GT2014-26252.
- [7]. Borello, D., Delibra, G., Andreini, A., Bianchini, C., 2012, "Unsteady CFD analysis of turbulent flow and heat transfer in a gas turbine blade trailing edge subjected to rotation", *Turboexpo 2012, Copenhagen, Denmark*.
- [8]. Borello D., D'Angeli L., Salvagni A., Venturini P., Rispoli F., "Study of particle deposition in gas turbine blades in presence of film cooling", *ASME Turbo Expo 2014, Dusseldorf, Germany*, paper no. GT2014-26250.
- [9]. Borello D., Rispoli F., Venturini P., "An integrated particle-tracking impact/adhesion model for the prediction of fouling in a subsonic compressor", *Journal of Engineering for Gas Turbine and Power*, 2012;134(9) (doi: <http://dx.doi.org/10.1115/1.4006840>).
- [10]. Venturini P., Borello D., Hanjalić K., Rispoli F., 2012, "Modelling of particle deposition in an environment relevant to solid fuel boilers", *Applied Thermal Engineering* 49, pp. 131-138.
- [11]. Tabakoff W., Kotwal R., Hamed A., 1979, "Erosion study of different materials affected by coal ash particles", *Wear*, 52, pp. 161-173.
- [12]. Corsini A., Rispoli F., Venturini P., Sheard A.G., "Numerical simulation of coal-fly ash erosion in an induced draft fan. *ASME Journal of Fluids Engineering*", 2013;135, paper 081303, pp. 1-12 (DOI: 10.1115/1.4024127).
- [13]. Corsini A., Marchegiani A., Rispoli F., Venturini P., Sheard A.G., "Predicting blade leading edge erosion in an axial induced draft fan". *ASME Transactions, Journal of Engineering for Gas Turbine and Power*, 2012;134(4) (doi: 10.1115/1.4004724).
- [14]. Cardillo L., Corsini A., Delibra G., Rispoli F., Sheard A.G., Venturini P., "Simulation of particle-laden flows in a large centrifugal fan for erosion prediction", *ASME Turbo Expo 2014, Dusseldorf, Germany*, paper no. GT2014-25865.
- [15]. Borello, D. and Orlandi, P., 2011, "DNS scrutiny of the elliptic-relaxation eddy viscosity model in channel flows with a moving wall", *Flow, Turbulence and Combustion*, Springer, 86, pp.295-309.
- [16]. Pettersson Reif, B. A., 2006, "Towards a nonlinear eddy-viscosity model based on elliptic relaxation", *Flow Turbulence Combust* 76, pp. 241-256.
- [17]. Pettersson Reif, B. A., Durbin, P. A., Ooi, A., 1999, "Modeling rotational effects in eddy-viscosity closures", *International Journal of Heat and Fluid Flow* 20, pp. 563-573.
- [18]. Sommerfeld, M., van Wachem, B., Oliémans, R., 2009, "Dispersed turbulent multi-phase flow. Best practice guide-lines", *ERCOFTAC*.